RECENT RESULTS IN INCLUSIVE CHARGED-CURRENT NEUTRINO-NUCLEAR SCATTERING

By M. Holder**

CERN, Geneva

(Received October 14, 1978)

Recent experiments on high energy neutrinos and antineutrinos from SPS and FNAL accelerators are discussed and compared with theoretical predictions.

1. Introduction

Neutrino and antineutrino interactions with nucleons are important for the determination of the internal structure of the proton and the neutron. They complement the deep inelastic electron or muon scattering experiments, which were the first to reveal point-like structures inside the nucleon. Whereas electron scattering experiments are sensitive to the average squared electric charge of the nucleon constituents, neutrino experiments measure their weak coupling. Different information is obtained in neutrino and antineutrino experiments owing to the parity violation in the weak interaction. This allows, in the language of the quark parton model, the separate measurement of the distribution of quarks and antiquarks in the nucleon.

Experimentation with high-energy neutrinos and antineutrinos from the SPS and FNAL accelerators has considerably widened the range of available momentum transfers in neutrino-nucleon interactions. Also the systematic uncertainties in cross-section measurements have been greatly reduced in the more recent experiments owing to the use of narrow-band neutrino beams. In this lecture the present status of experiments and their comparison with theoretical predictions is summarized. In Section 2 we recall the formal description of neutrino-nucleon scattering; in Section 3 a very brief account of narrow-band beams and detectors is given; experimental results are presented in Section 4, and

* Presented at the XVIII Cracow School for Theoretical Physics, Zakopane, May 27-June 8, 1978.

** Present address: II. Institut f. Experimentalphysik, Luruper Chaussee 149, 2000 Hamburg 50, West Germany.

summarized in Section 5. For a more detailed review of the experimental apparatus and for a discussion of the older results the reader is referred to the Wépion lectures [1] of Steinberger.

2. *Theoretical description of neutrino interactions*

2.1. The most general form of the cross-section

The cross-sections for the inclusive reactions $\nu+N \to \mu^-+X$ and $\bar{\nu}+N \to \mu^++X$ of neutrinos or antineutrinos on an isoscalar target $N = \frac{1}{2}(n+p)$ are traditionally calculated from an interaction Lagrangian, which is the product of a leptonic and a hadronic current

$$L = \frac{G}{\sqrt{2}} J_l^\alpha J_h^\alpha.$$

The leptonic current is known from β-decay experiments; the hadronic current is unknown. The cross-section is calculated from first-order perturbation theory and has the general form [2]

$$\frac{d\sigma^{\nu,\bar{\nu}}}{dxdy} = \frac{G^2 ME}{\pi}\left[\left(1-y-\frac{xyM^2}{s}\right)F_2^{\nu,\bar{\nu}} + y^2 xF_1^{\nu,\bar{\nu}} \pm \left(y-\frac{y^2}{2}\right)xF_3^{\nu,\bar{\nu}}\right], \tag{1}$$

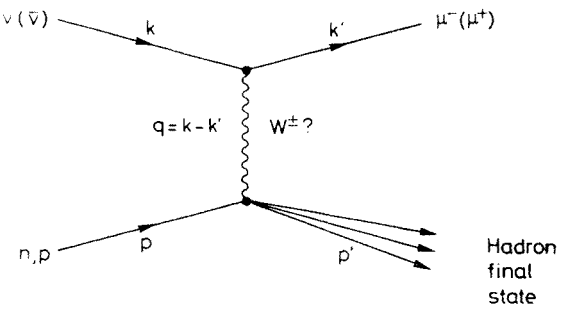

Fig. 1. Feynman diagram for inclusive neutrino-nucleon scattering

where G is the Fermi coupling constant, x and y are dimensionless variables formed from the relativistic invariants of the process (see Fig. 1)

$$x = \frac{Q^2}{2Mv}, \quad y = \frac{v}{E}, \quad Q^2 = -q^2, \quad v = \frac{p\cdot q}{M},$$

E is the neutrino energy in the laboratory system, and $F_i^{\nu,\bar{\nu}}(Q^2, v)$ $(i = 1, 2, 3)$, are structure functions to be determined experimentally.

If the weak interaction is mediated by an intermediate boson W, the cross-sections have the same form, except that the structure functions have to be multiplied by the factor $1/(1+Q^2/M_W^2)^2$, the square of the W-propagator term.

It may be worth mentioning that higher order corrections contain infinities. These infinities are avoided by gauge theories of weak and electromagnetic interactions.

2.2. Special assumptions

2.2.1. The scaling hypothesis

The scaling hypothesis is the conjecture [3] that at high Q^2 and ν the structure functions depend only on the single dimensionless variable x. In the absence of any cut-offs the total cross-sections rise then linearly with energy. In the case of exchanged intermediate bosons, the W-propagator term keeps the cross-sections finite.

2.2.2. Spin $\frac{1}{2}$ constituents

If one assumes that scaling is valid and that interactions occur in fact on constituents of the nucleon which have spin $\frac{1}{2}$, there is a relation (the Callan–Gross relation [4]) between the structure functions:

$$2xF_1(x) = F_2(x). \tag{2}$$

In this case the cross-section formula simplifies to

$$\frac{d\sigma^{\nu,\bar{\nu}}}{dxdy} = \frac{G^2ME}{2\pi}\{[1+(1-y)^2]F_2^{\nu,\bar{\nu}} \pm [1-(1-y)^2]xF_3^{\nu,\bar{\nu}}\}. \tag{3}$$

The y-dependence contains then only a constant and a $(1-y)^2$ term, the linear term being proportional to $F_2 - 2xF_1$. In other words, a term proportional to $(1-y)$ signals the violation of the Callan–Gross relation.

Similar arguments apply for electroproduction experiments. In these one can measure the ratio between longitudinal and transverse virtual photon cross-sections:

$$R = \frac{\sigma_L}{\sigma_T} = \frac{F_2}{2xF_1}\left(1 + \frac{Q^2}{\nu^2}\right) - 1, \tag{4}$$

which should vanish in the limit of high Q^2 and ν, if the Callan–Gross relation holds.

2.2.3. Charge symmetry

For strangeness-conserving transitions one assumes that the form factors are isospin symmetric: $F_i^{\nu p} = F_i^{\bar{\nu} n}$ and $F_i^{\bar{\nu} p} = F_i^{\nu n}$, such that $F_i^{\nu N} = F_i^{\bar{\nu} N}$ for isoscalar targets. Especially, neutrino and antineutrino cross-sections should be equal for $y = 0$, where the vector axial-vector interference term (the last term in Eq. (1)) vanishes:

$$\left.\frac{d\sigma^{\nu}}{dy}\right|_{y=0} = \left.\frac{d\sigma^{\bar{\nu}}}{dy}\right|_{y=0} = \frac{G^2ME}{\pi} F_2. \tag{5}$$

2.2.4. The quark parton model

In the quark parton model the neutrino and antineutrino reactions are the sum of elementary reactions on quarks and antiquarks. For a $V-A$ coupling the reactions of neutrinos on quarks and the reactions of antineutrinos on antiquarks have isotropic angular distributions in the neutrino–quark centre-of-mass system, which translate into a flat y-distribution in the laboratory system, and the reactions of neutrinos on quarks

as well as those of antineutrinos on antiquarks are proportional to $(1-y)^2$. Some elementary reactions and their cross-sections are [5]

Reaction	$\frac{\pi}{G^2ME}\frac{d\sigma}{dxdy}$
$\nu+d \to \mu^-+u$	$2xd(x)\cos^2\theta_c$
$\nu+d \to \mu^-+c$	$2xd(x)\sin^2\theta_c$
$\bar{\nu}+u \to \mu^++d$	$2xu(x)(1-y)^2\cos^2\theta_c$
$\bar{\nu}+d \to \mu^++c$	$2xd(x)(1-y)^2\sin^2\theta_c$
$\bar{\nu}+u \to \mu^++s$	$2xu(x)(1-y)^2\sin^2\theta_c$
$\nu+s \to \mu^-+u$	$2xs(x)\sin^2\theta_c$

where $u(x)$, $d(x)$, $s(x)$ and $c(x)$ are, respectively, the densities of up, down, strange, and charmed quarks in the proton and θ_c is the Cabibbo angle. With the abbreviation $q = u+d+s+c$ and $\bar{q} = \bar{u}+\bar{d}+\bar{s}+\bar{c}$ the cross-sections per nucleon on an isoscalar target are, for masses of the hadronic recoil system well above charm threshold,

$$\frac{d\sigma^{\nu}}{dxdy} = \frac{G^2ME}{\pi}x[q+s-c+(1-y)^2(\bar{q}-\bar{s}+\bar{c})],$$

$$\frac{d\sigma^{\bar{\nu}}}{dxdy} = \frac{G^2ME}{\pi}x[\bar{q}+\bar{s}-\bar{c}+(1-y)^2(q-+c)]. \tag{6}$$

If one compares Eq. (5) with the general form (Eq. (2)) of the cross-section, one obtains the following correspondence between the form factors and the quark densities:

$$F_2^{\nu} = F_2^{\bar{\nu}} = q+\bar{q}, \quad xF_3^{\nu} = q-\bar{q}+2(s-c), \quad xF_3^{\bar{\nu}} = q-\bar{q}-2(\bar{s}-\bar{c}). \tag{7}$$

It is interesting to note that the form factor xF_3 is not charge-symmetric, i.e. $xF_3^{\nu} \neq xF_3^{\bar{\nu}}$, if the densities of strange and charmed quarks in the nucleon are different. The average of xF_3^{ν} and $xF_3^{\bar{\nu}}$ gives the distribution of valence quarks:

$$xF_3 = \tfrac{1}{2}(xF_3^{\nu}+xF_3^{\bar{\nu}}) = q-\bar{q}. \tag{8}$$

For the same reason the ratio of antiquarks to quarks plus antiquarks, as determined from the coefficients in the y-distributions, is expected to be different for neutrino and antineutrino reactions. In neutrino reactions one measures $\frac{\bar{q}-s+c}{q+\bar{q}}$, in antineutrino reactions $\frac{\bar{q}+\bar{s}-\bar{c}}{q+\bar{q}}$.

2.2.5. Relation to electron-nucleon scattering

In the quark parton model the cross-section for electron-nucleon scattering is given by [5]

$$\frac{d^2\sigma^{eN}}{dxdy} = \frac{4\pi\alpha^2}{Q^4}ME[1+(1-y)^2]\left[\tfrac{5}{18}(u+d+\bar{u}+\bar{d})+\tfrac{1}{9}(s+\bar{s})+\tfrac{4}{9}(c+\bar{c})\right], \tag{9}$$

where u, d, s, and c are the usual quark densities. Since the x-distributions of s and c quarks are different from those of u and d quarks, the coupling constant is x-dependent. If one ignores the effect of c quarks and the difference between the coupling of s and u or d quarks, one expects

$$F_2^{eN}(x) = \tfrac{5}{18} F_2^{\nu N}(x). \tag{10}$$

Especially $\int F_2^{\nu N}(x)dx = 3.6 \int F_2^{eN}(x)dx$. For the SLAC data $\int F_2^{eN}(x)dx = 0.14 \pm 0.005$ [6], which gives the prediction $\int F_2^{\nu N}(x)dx = 0.50 \pm 0.02$.

2.2.6. Scaling deviations

Deviations from scaling are expected at high Q^2 in any field theory of strong interactions. The reason is that essentially two processes occur which suppress the cross-section at high x (high quark momenta) and enhance the low x cross-section (see Fig. 2):

a) the quark which participates in the weak interaction radiates a field quantum (gluon) before it interacts;

b) a gluon creates a quark-antiquark pair, and the weak interaction takes place at one of these "sea" quarks.

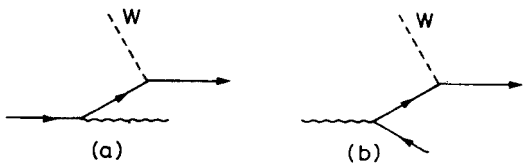

Fig. 2. Neutrino-quark scattering diagrams in the presence of gluons. In (a) the gluon is radiated before the quark interacts with the virtual W, in (b) a quark-antiquark pair is created by a gluon and the W interacts with one of the members of the pair

Quantitative predictions for the change with Q^2 of the structure functions are given by Quantum Chromodynamics (QCD). Provided the moments of the quark, antiquark, and gluon distribution functions are known for a given Q_0^2, they can be calculated at any other Q^2.

The QCD equations are particularly simple for the moments of the valence quark distribution. If one denotes the distribution function of valence quarks as $V(x, Q^2)$ and defines the n^{th} moment as

$$V_n(Q^2) = \int x^{n-1} V(x, Q^2)dx$$

the Q^2-dependence according to QCD, is given by

$$V_n(Q^2) = V_n(Q_0^2) \exp(-s\gamma^n), \tag{11}$$

where

$$s = \log\left[\frac{\log(Q^2/\Lambda^2)}{\log(Q_0^2/\Lambda^2)}\right], \quad \gamma^n = \frac{4}{33-2m}\left[1 - \frac{2}{n(n+1)} + 4\sum_{j=2}^{n}\frac{1}{j}\right],$$

and m is the number of quark flavours ($m = 4$, if one counts up, down, strange, and charmed quarks).

The only free parameter in this theory is Λ. It defines a scale in Q^2. The expected variations are logarithmic in Q^2. The effects are therefore most pronounced for Q^2 less than or of the same order as Λ^2. A consequence of Eq. (11) is that two moments should be related by a simple power law

$$\frac{\partial \ln V_n(Q^2)}{\partial \ln V_m(Q^2)} = \frac{\gamma_n}{\gamma_m}. \tag{12}$$

This can be tested experimentally.

3. Neutrino beams and detectors

3.1. Narrow-band beams

An important alternative to the conventional horn-focused wide-band beams is the so-called narrow-band neutrino beam. It is formed from a parallel beam of momentum--selected secondary particels which decay. If γ is the Lorentz factor of the secondaries, the neutrino energy in a two-body decay $\pi \to \mu\nu$ or $K \to \mu\nu$ is determined by the decay angle θ between the neutrino and the parent particle. For small angles

$$E_\nu = \frac{E_{\max}}{1+\gamma^2\theta^2}, \tag{13}$$

where

$$E_{\max} = E_{\pi,K}\left(1 - \frac{m_\mu^2}{m_{\pi,K}^2}\right).$$

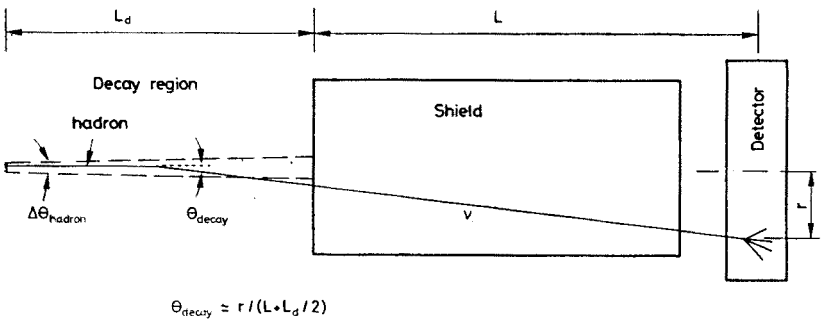

Fig. 3. Relation between decay angle and radial position of a neutrino event in a detector

Conversely, for fixed angle θ the neutrino energy is known except for the π/K ambiguity. The decay angle θ can be approximetely determined from the radial position of an event in the detector (Fig. 3). In both bubble chamber and counter experiments, the total energy of charged current events is actually measured as the sum of muon and hadron energies. The comparison with the neutrino energy, as computed from Eq. (13), is, however, an important check. In the study of neutral current events the a priori knowledge of the neutrino energy is crucial.

A second advantage of the narrow-band beam is that the neutrino *spectrum* is well known. From two-body decays of monochromatic parents one obtains a flat spectrum. In large radius detectors (large θ acceptance), as for the CERN experiments, the full spectrum from zero to 95% of the parent beam energy is obtained with the same beam setting (see Fig. 4). The neutrino flux is determined by measurement of only two parameters: the K/π ratio and the total $(K+\pi)$ intensity. The K/π ratio (and the K/p ratio in the positive

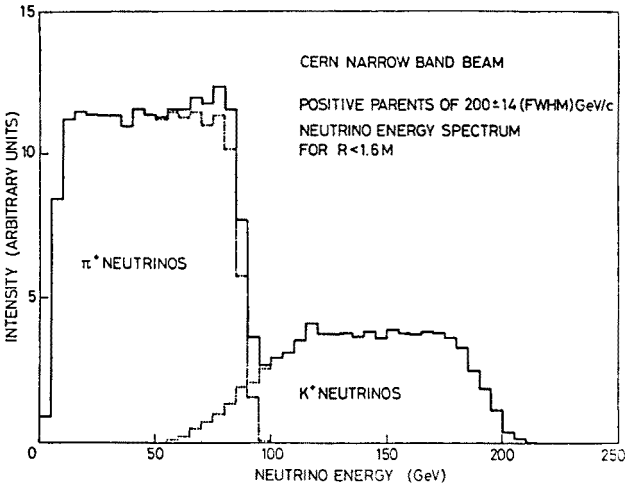

Fig. 4. Neutrino spectrum in the CDHS detector

beam) is measured by a differential Cerenkov counter. For the total flux measurements various techniques are applied, such as beam current transformers, secondary emission chambers, ion chambers, solid-state detectors in the muon shield, etc. Imperfections in the flux-measuring technique result in uncertainties in the absolute cross-section; they do *not* influence the shape of the neutrino spectrum. The energy dependence of the cross-section measured in the same beam is therefore better known than the absolute value of the cross-section. The only flux uncertainty which comes into play is the error in the K/π ratio.

3.2. Detectors

Neutrino detectors are very massive owing to the smallness of the neutrino cross-section. Target masses range from a few tons for bubble chambers up to more than 1000 tons for counter experiments. The bubble chambers (the 15 ft chamber at FNAL, BEBC and Gargamelle (GGM) at CERN) have the traditional advantage that they show in detail the secondary particles created in an interaction. All chambers used in neutrino physics are equipped with external muon identifiers, i.e. wire chambers which identify muons from penetration through the iron yoke of the magnet and additional material. The detection and correct assignment of neutral particles, especially π^0's, presents a problem for bubble chambers. It is solved in various ways. In the BEBC narrow-band beam

experiment, for example, the total observed hadronic energy was found to be 20% lower than the true hadronic energy, from transverse momentum balance. A 20% correction to the measured hadron energy was therefore applied in all events. The resulting error on the hadron energy was estimated to be 20% r.m.s.

The error on the muon momentum in the BEBC experiment is 4% r.m.s. at 100 GeV/c.

The counter experiments are designed to measure muon momentum and angle, and the total energy of all hadrons. The instrumentation consists of a muon spectrometer and a total absorption calorimeter. Most calorimeters are constructed as iron scintillator sandwiches. The scintillators take sample of the hadron shower which develops mainly

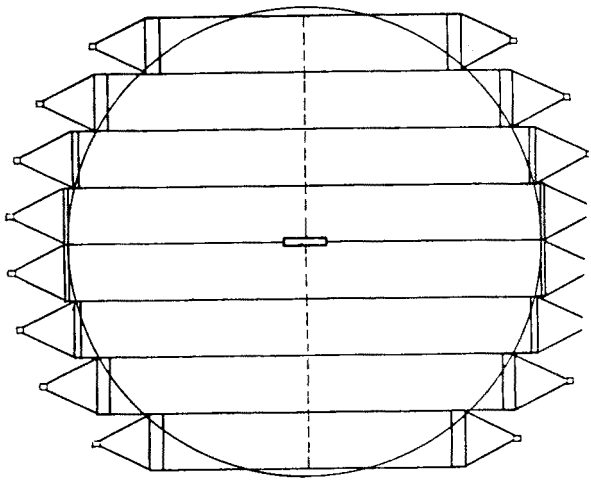

Fig. 5. Front view of a module of the CDHS experiment. Horizontal strips of scintillators with light guides at both ends are sandwiched between iron disks of 3.85 m diameter

in the iron. In the CERN–Dortmund–Heidelberg–Saclay (CDHS) experiment [7] the functions of muon spectrometer and hadron calorimeter are combined using magnetized iron for the sandwiches. Iron disks of 5 cm or 15 cm thickness with a central hole are sandwiched with scintillators and combined in toroidal modules of 75 cm Fe thickness (see Fig. 5). The modules are magnetized by coils which pass through the central hole. The hadron energy resolution in such a calorimeter depends on the energy. It improves with energy and was found to be $(\Delta E/E)_{\text{rms}} = 0.86/\sqrt{E}/\text{GeV}$ for 5 cm iron plates [8]. This means that at 100 GeV the resolution is as good as 8.6%, below 10 GeV it is more than 30%.

The measurement accuracy of muon momenta in iron toroids is determined by multiple scattering. In the CDHS experiment, $\Delta p_\mu/p_\mu \approx 10\%$, independent of the muon momentum. The measurement of the muon angle is limited by the undetected multiple scattering in the iron between the origin of an event and the first usable wire chamber. The CDHS figure is $\Delta\theta \cdot p_\mu = 0.16$ GeV/c.

Owing to these measurement errors the observed distributions are different from the true distributions. In the presentation of the data the observed distributions are usually

corrected for the effect of measurement errors. With the above figures the corrections are normally less than 20%. If they are larger (e.g. for $x > 0.6$) the systematic error due to the uncertainty in the measurement errors may be non-negligible.

In both bubble chamber and counter experiments, a minimum energy is required for the muon. The data are corrected for the loss of events due to this cut, when necessary, by estimating the effect of the cut with simulated events.

4. Results

The more accurate results on inclusive charged current cross-sections have been obtained by groups working in narrow-band beams: the CalTech Fermi Lab (CITF) Collaboration at FNAL, the BEBC group and the CDHS Collaboration at CERN. The CDHS results are still preliminary at the time of this lecture and may be subject to minor modifications. The BEBC group has made an interesting analysis combining high-energy data with GGM data obtained at the PS neutrino beams. Some of these results will be reported below.

4.1. Total cross sections

Total cross sections are obtained from a measurement of the charged current event rate as a function of neutrino energy and from a measurement of the neutrino flux as discussed in Section 3.1. Results are presented in Fig. 6 for the BEBC/GGM [9–12] and

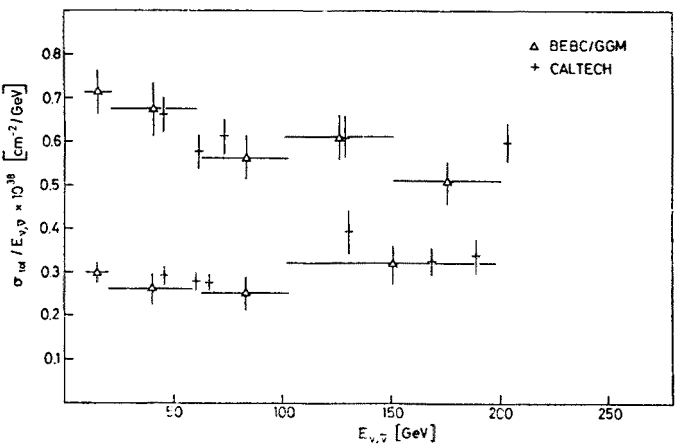

Fig. 6. Total cross-section measurements. The error bars include systematic errors

CITF [13] groups and in Fig. 7 for the CDHS [14] group. The CDHS data have an overall scale error due to the absolute flux normalization of $\pm 5\%$ in addition to the errors shown in Fig. 7, i.e. all the data points may have a common displacement by $\pm 5\%$. Moreover, the data point above 90 GeV have an additional $\pm 10\%$ systematic error compared with the points below 90 GeV owing to a 10% uncertainty in the K/π ratio. Taking these points

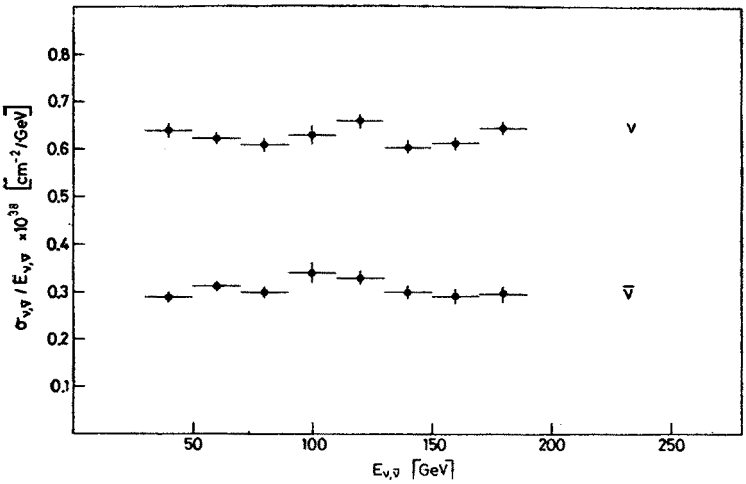

Fig. 7. Total cross-sections measured by the CDHS group. The error bars do not include a common scale error of 5% or a common ±10% displacement of the points above 90 GeV owing to the uncertainty in the K/π ratio

into account, one concludes that

(*i*) The neutrino cross-section per unit energy (σ/E) decreases from its value at PS energies (< 10 GeV); the σ/E for antineutrinos is constant within 10%.

(*ii*) Between 40 GeV and 180 GeV, σ/E for both ν and $\bar{\nu}$ changes less than 10%; it is compatible with being constant.

This is also illustrated by the energy dependence of the cross-section ratio (Fig. 8), as obtained by the CDHS group. A constant value of σ/E is expected if Bjorken scaling

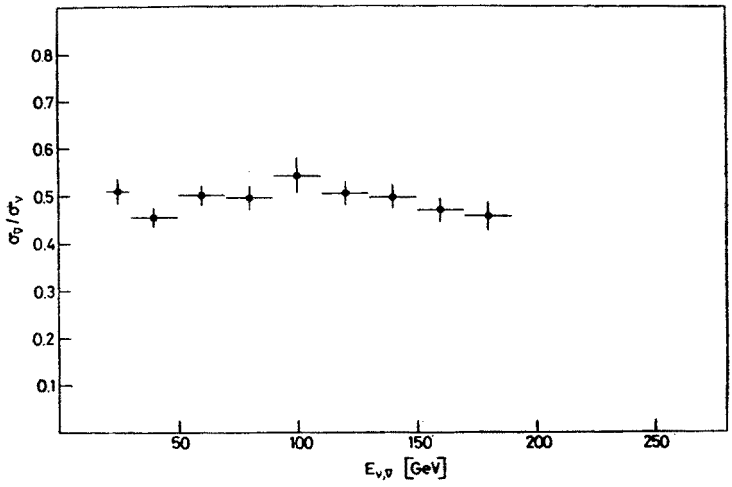

Fig. 8. $\bar{\sigma}^{\nu}/\sigma^{\nu}$ from CDHS. The data above 90 GeV have a common systematic error of ±10% compared with the points below 90 GeV, not included in the figure

holds. Asymptotically free field theories predict an increase of 5% in the $\bar{\nu}/\nu$ cross-section ratio between 40 GeV and 180 GeV [15], certainly compatible with the data. Improvements, for example in the K/π ratio, are needed, before such small effects are really measurable.

4.2. *y*-distributions

The inclusive cross-sections are functions of three variables, say, x, y, E, or x, y, Q^2 (they are related by $Q^2 = 2MxyE$). Experimentally it is convenient to study y-distributions at fixed neutrino energy, integrating the form factors in x from 0 to 1. Another choice would be to fix Q^2, with the disadvantage that the available x-range depends on y because

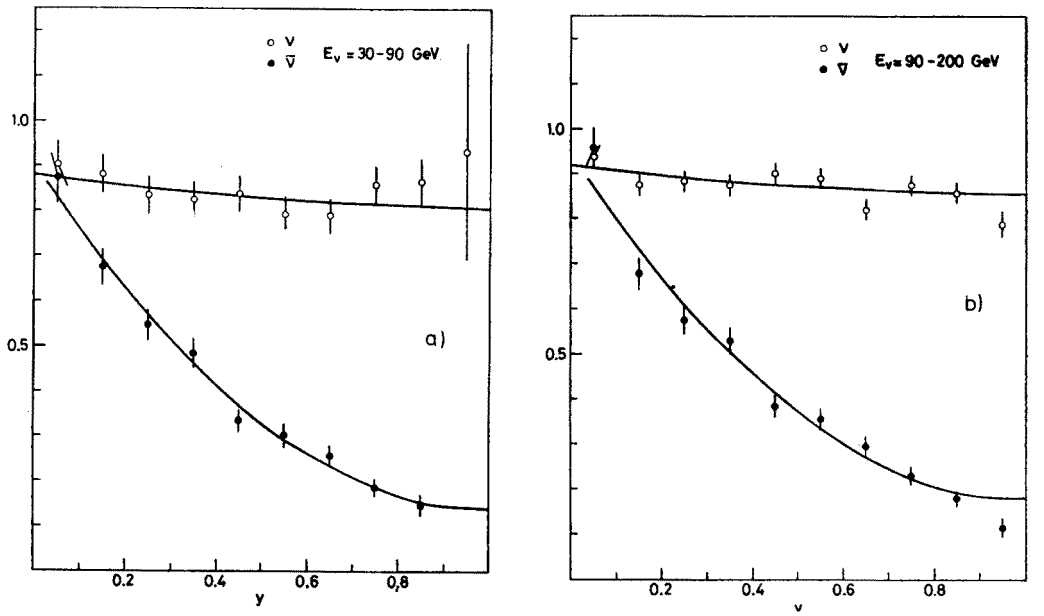

Fig. 9. y-distributions, corrected for acceptance and resolution effects, from CDHS

of the limitation in neutrino energy. Another advantage of distributions at fixed energy is that they are not affected by uncertainties in the ν-spectrum.

Neutrino and antineutrino y-distributions, normalized to the same flux, from the CDHS experiment are shown in Fig. 9 for the energy ranges $30 < E < 90$ GeV and $90 < E < 200$ GeV. They contain information on the following issues:

(*i*) *Callan–Gross relation* (Eq. (3)). A term in the y-distribution proportional to $(1-y)$ indicates a non-vanishing value of $\delta = 1 - \int 2xF_1(x)dx / \int F_2(x)dx$. From a fit to the y-distribution the CDHS group obtains $\delta = (-2 \pm 3)\%$. By positivity conditions $\delta > 0$, which allows the setting of an upper limit of $\delta < 5\%$. No radiative corrections have been applied. According to present estimates these will increase δ to a value of less than 10%. The result of the BEBC experiment [12] is $\delta = 0.11 \pm 0.12$, also not including radiative corrections. These values may be compared with the measurement of R

in inelastic electron scattering $R = 0.2 \pm 0.1$, which corresponds approximately to $\delta = 0.10 \pm 0.10$. A non-zero value of δ of this order is expected in QCD.

(*ii*) *Charge symmetry*. The differential cross-sections for neutrino and antineutrino reactions at $y = 0$

$$f^{\nu,\bar{\nu}} = \frac{1}{E} \frac{d\sigma^{\nu,\bar{\nu}}}{dy}\bigg|_{y=0}$$

should be equal according to Eq. (5). The experimental results (Table I) support this conjecture.

TABLE I

Forward scattering cross-sections $f^{\nu,\bar{\nu}} = \frac{1}{E} \frac{d\sigma^{\nu,\bar{\nu}}}{dy}\Big|_{y=0}$

$f^{\nu,\bar{\nu}}$ in 10^{-38} cm^2/GeV	$\int F_2\, dx$	E-range/GeV	Group	Ref.
$f^{\nu} = 0.77 \pm 0.06 - (0.66 \pm 0.65) \times 10^{-3}\, E/\text{GeV}$ $f^{\bar{\nu}} = 0.75 \pm 0.06 - (0.24 \pm 0.50) \times 10^{-3}\, E/\text{GeV}$	0.46 ± 0.02	$45 < E < 205$	CITF	[17]
$f^{\bar{\nu}}/f^{\nu} = 1.1 \pm 0.2$ $\frac{1}{2}(f^{\nu}+f^{\bar{\nu}}) = 0.79 \pm 0.07$	0.51 ± 0.05	$20 < E < 200$	BEBC	[11]
$f^{\bar{\nu}}/f^{\nu} = 1.05 \pm 0.07$ 1.06 ± 0.11	0.44 ± 0.03 0.47 ± 0.05	$30 < E < 90$ $90 < E < 200$	CDHS	[14]

(*iii*) *Momentum in quarks and antiquarks*. Quarks and antiquarks carry the fraction $\int [q(x)+\bar{q}(x)]dx = \int F_2(x)dx$ of the nucleon momentum. This is related to the cross-section at $y = 0$ by Eq. (5). The values of $\int F_2 dx$ obtained in this way are listed in Table I. They are about 10% to 20% lower than the value expected from electron–deuteron scattering under the assumption of scaling (see Section 2.3.4). A more detailed comparison of the Q^2-dependence of form factors, presented in Section 4.4, shows that at least part of this descrepancy is probably due to scaling violations.

(*iv*) *Antiquark/quark ratio*. From the coefficients of the y-distributions in neutrino and antineutrino reactions, the CDHS group obtains, using Eq. (6)

$$\frac{\bar{q}-s+c}{q+\bar{q}} = 0.08+0.04, \qquad \frac{\bar{q}+\bar{s}-\bar{c}}{q+\bar{q}} = 0.16+0.02,$$

averaged over the neutrino spectrum in the energy range $30 < E < 200$ GeV. The average value of ν and $\bar{\nu}$ data is $\bar{q}/(q+\bar{q}) = 0.12 \pm 0.02$, in good agreement with the average value from BEBC [12] $\bar{q}/(q+\bar{q}) = 0.11+0.03$. The difference between ν and $\bar{\nu}$ data is as expected in the quark model for an SU(3) symmetric sea with $s = \bar{s} = \bar{u} = \bar{d}$ and $c = \bar{c} = 0$. It is also compatible with a somewhat smaller density of strange quarks as suggested, for example, by the analysis of dimuon events [16].

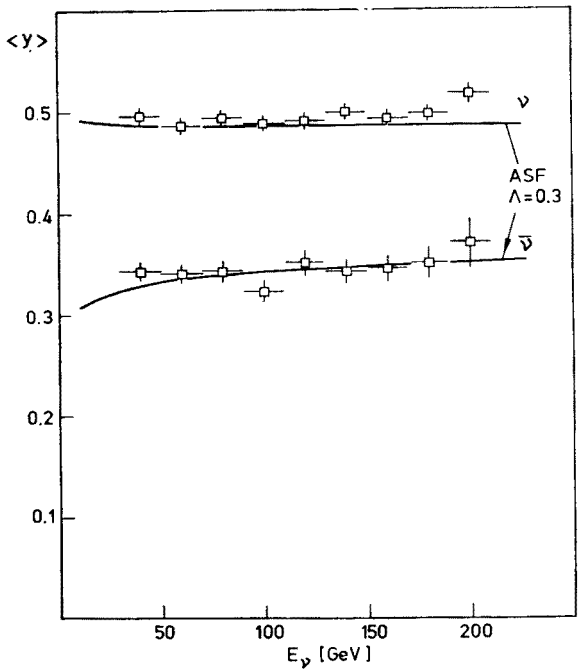

Fig. 10. $\langle y \rangle$ versus energy from CDHS

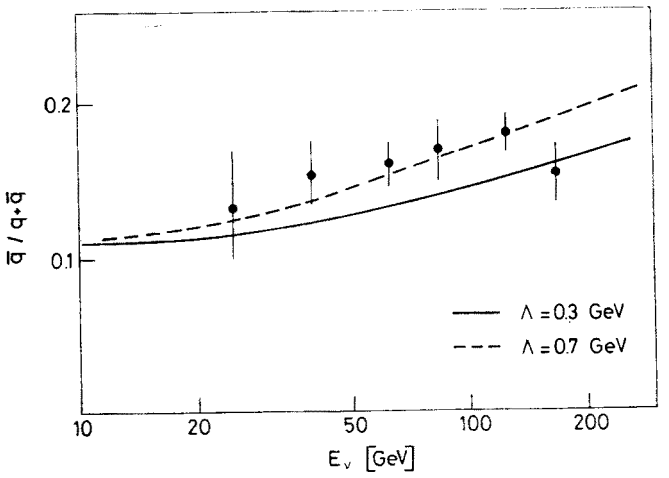

Fig. 11. Fraction of antiquarks as a function of total energy from CDHS. The curves indicate the change expected in QCD

In the energy range between 30 GeV and 200 GeV the ratio of antiquarks to quarks is compatible with being constant. This is illustrated in Fig. 10, which shows the first moment of the y distributions from CDHS, and in Fig. 11 which gives the $(\bar{q}+\bar{s}-\bar{c})/(q+\bar{q})$ ratio determined from the ratio of $\bar{\nu}$ to ν cross-sections at high y by the same group. It should be pointed out that the data is *also* compatible with a change of the $\bar{q}/(q+\bar{q})$ ratio as required by QCD. Slightly different results were obtained by the CITF group [18]. They see no energy dependence from 45 to 205 GeV in $\langle y\rangle^{\nu}$, but a $(10\pm5)\%$ increase in $\langle y\rangle^{\bar{\nu}}$ between the high-energy ($\approx$ 160 GeV) and the low-energy ($\approx$ 60 GeV) data. Their averages are $\langle y\rangle^{\nu} = 0.47+0.01$ and $\langle y\rangle^{\bar{\nu}} = 0.32+0.01$. The observed increase in $\langle y\rangle^{\bar{\nu}}$ corresponds to an increase in the $(\bar{q}+\bar{s}-\bar{c})/(q+\bar{q})$ ratio from 0.08 ± 0.03 to to 0.14 ± 0.03.

4.3. x-distributions

One of the expectations of the quark model is that x-distributions at high y are different in neutrino and antineutrino reactions. High y neutrino reactions probe essentially the distribution of quarks, antineutrino reactions that of antiquarks. As shown by the

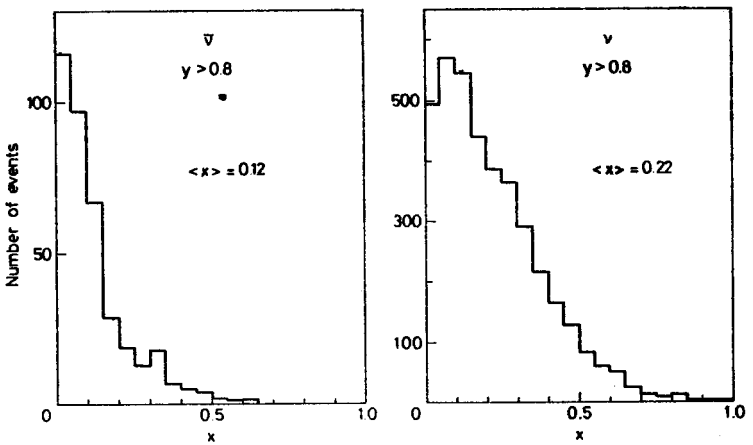

Fig. 12 x-distributions for $y > 0.8$ from CDHS

data with $y > 0.8$ from the CDHS group (Fig. 12), there is in fact a clear difference in the distributions; antiquarks are more concentrated at low x. A more accurate determination of the relative amount of quarks and antiquarks as a function of x is provided by fits to the y-distributions in bins of x, following Eq. (16). The result from CDHS is shown in Fig. 13. If the valence-quark and the antiquark distributions are parametrized by

$$xF_3(x) \propto \sqrt{x}\,(1-x)^n$$

and

$$\bar{q}(x) \propto (1-x)^m$$

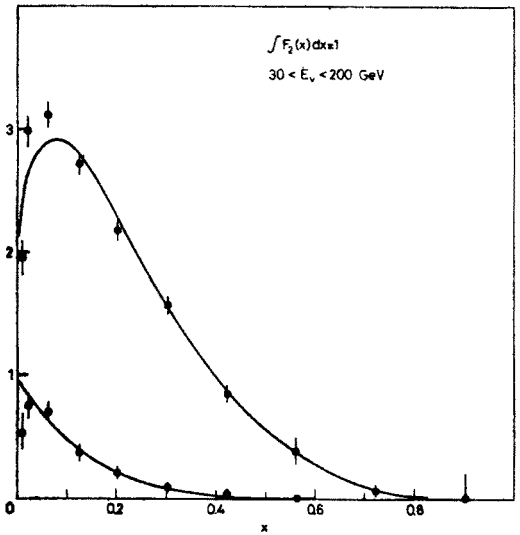

Fig. 13. Average x-distributions for $F_2(x)$ (upper points) and $\bar{q}(x)$ (lower points) from CDHS. The curves are fits to the form $F_2(x) = \sum_{n=3}^{7} a_n(1-x)^n$ and $\bar{q}(x) = \sum_{n=6}^{7} b_n(1-x)^n$

the best fit values for the exponents are $n = 3.5 \pm 0.5$ and $m = 6.7 \pm 0.5$. Similar results were obtained by the BEBC group (Fig. 14). They find that the quark distribution is characterized by a $(1-x)^3$ behaviour for $x > 0.3$ and that the antiquark distribution can be described by $\bar{q}(x) \propto (1-x)^m$ with $m = 4.9^{+2.4}_{-1.7}$.

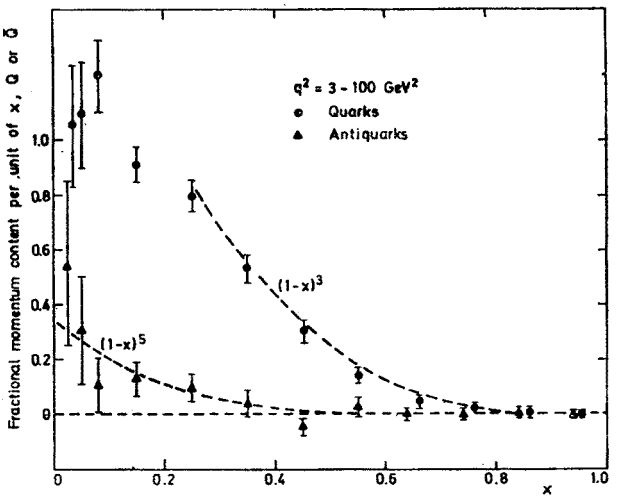

Fig. 14. Average x-distributions from the BEBC-GGM experiment

The expectation that at $x = 0$ the momentum carried by quarks and antiquarks is the same, or in other words that $F_2(0) = q(0) + \bar{q}(0) = 2\bar{q}(0)$, is compatible with the data, considering that the x-distribution is very steep near $x = 0$.

It is interesting to see how the x-distributions in inclusive charged current reactions are related to those in dimuon events. Opposite sign dimuon events seem to be mostly due to charmed particle production and decay [16]. In the quark model, antineutrino reactions occur only on "sea" quarks, neutrino reactions occur in roughly equal amounts on sea and valence quarks. The reactions are

$$\nu + d \to \mu^- + c \quad , \quad \nu + s \to \mu^- + c \quad , \quad \bar{\nu} + \bar{s} \to \mu^+ + \bar{c} \quad ,$$
$$\qquad\qquad \lfloor\!\to \mu^+ + \nu + s \qquad\qquad \lfloor\!\to \mu^+ + \nu + s \qquad\qquad \lfloor\!\to \mu^- + \bar{\nu} + \bar{s}$$

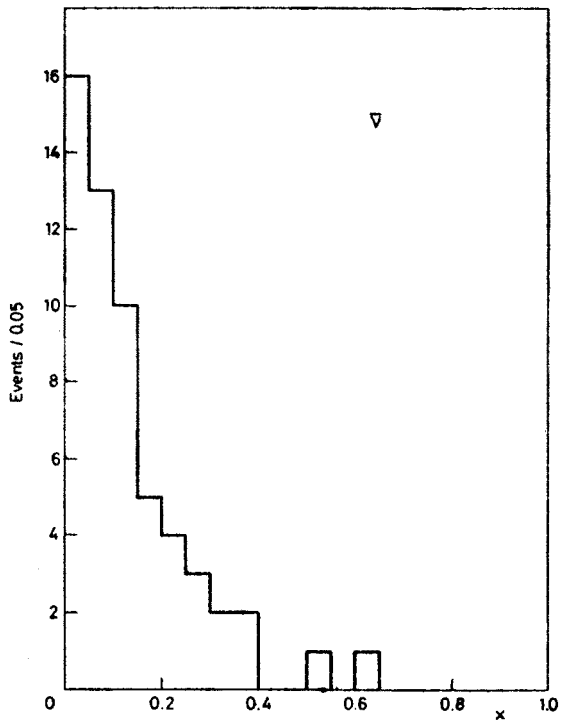

Fig. 15. x-distribution of opposite sign dimuon events in $\bar{\nu}$-reactions (from Ref. [16])

The CDHS data (Fig. 15) show in fact that the x-dependence of antineutrino dimuon reactions coincides with the momentum distribution of antiquarks, as measured in high y charged-current $\bar{\nu}$-reactions (Fig. 12); neutrino dimuon production has an x-dependence which falls between the quark and antiquark momentum distributions.

4.4. Scaling violations

A straightforward experimental test of scaling is to compare x-distributions at different neutrino energies. The CDHS data (Fig. 16) show, in fact, an energy dependence, most clearly for $F_2(x)$. The direction of the changes is as anticipated by theoretical arguments (see Section 2.2.6): the width of the distribution shrinks with increasing energy, which means increasing Q^2. This is a first evidence for scaling violations.

In a next step, guided by theoretical arguments, one would like to determine the

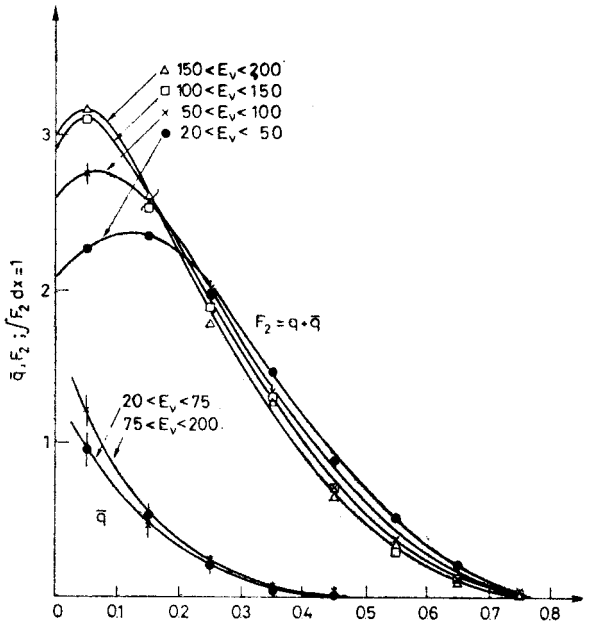

Fig. 16. x-distributions for various intervals of E_ν from CDHS

dependence of the form factors on x and Q^2. Data for F_2 and xF_3 from the BEBC-GGM group [11, 12] and for F_2 from CDHS [14] are presented in Figs. 17–19. All data show more or less pronounced scaling violations, depending on the x-value and the Q^2-range. The Q^2-dependence of the form factors is such that the biggest changes are observed at small Q^2, and only a modest variation, if any, is visible at high Q^2, in agreement with a log type behaviour. It is interesting now to compare these structure functions with those

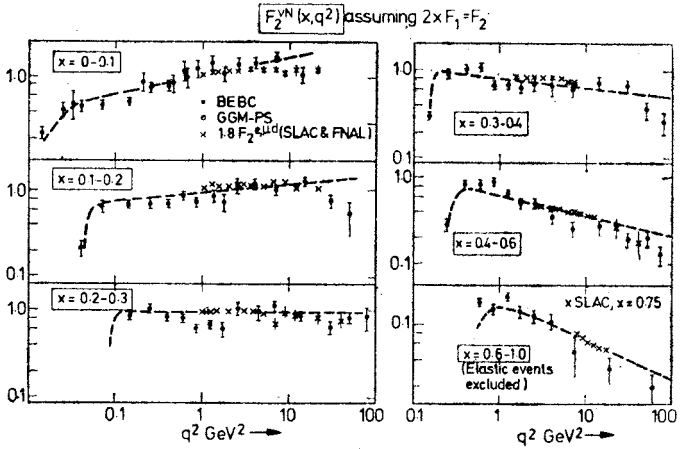

Fig. 17. BEBC–GGM results for $F_2(x, Q^2)$, with results from eN or μN scattering superimposed. The curves result from an empirical parametrization of scaling violations

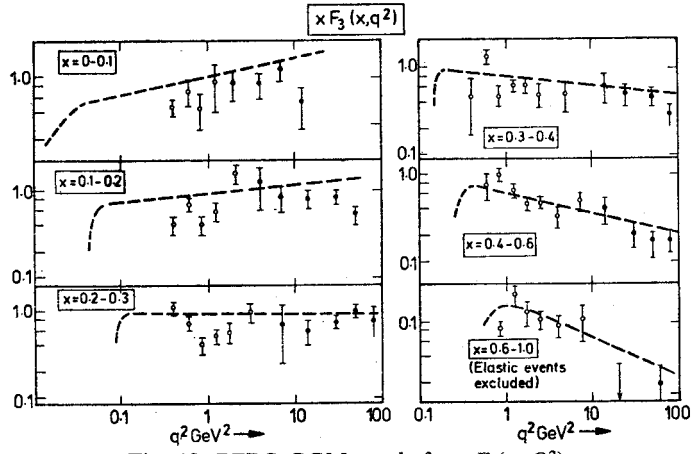

Fig. 18. BEBC–GGM result for $xF_3(x, Q^2)$

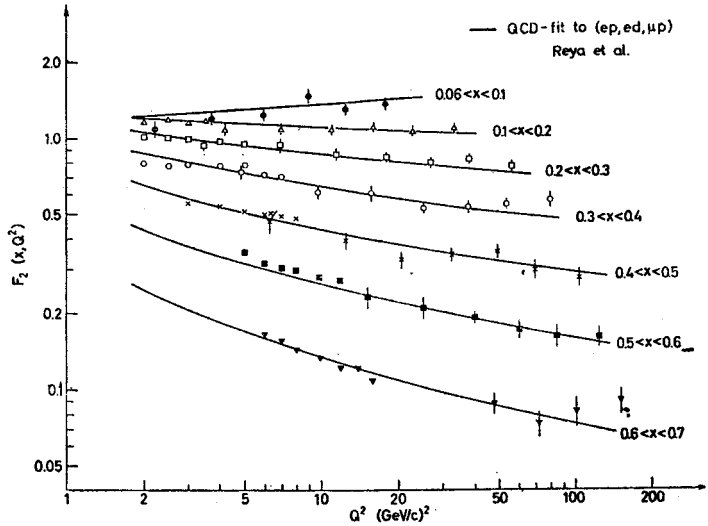

Fig. 19. CDHS result for $F_2(x, Q^2)$. Points without error bars are ed data (Ref. [19]), multiplied by 1.8. The curves are QCD fits to the eN and μN data ($\Lambda = 0.5$ GeV)

determined in eN scattering, and to see if the observed scaling violations check with theoretical predictions. We content ourselves here with a few remarks.

(*i*) *Comparison with ed scattering.* In the quark model neutrino- and electron-scattering experiments are related by Eq. (9). If the form factor $\frac{1}{2}F_2^{ed}(x, Q^2)$, measured in ed scattering [19], is multiplied by 18/5 (to be more correct, this factor should be x-dependent, see Section 2.3.4) it is in remarkable agreement (within 10%) with the form factor $F_2^{\nu N}(x, Q^2)$ in the Q^2-region where they overlap; the neutrino experiments have perhaps a tendency to give a lower value for F_2. This may be partly due to the fact that the threshold for charmed particle production is not yet reached. At high Q^2 the neutrino data continue the trend observed in the ed data.

(*ii*) *Comparison with QCD.* QCD fits to ed and μN data have been made by various authors [20–22]. In electron or muon experiments the antiquark distributions are not measurable. Using antiquark distributions as given by the CDHS experiment and ed data as input to QCD fits one obtains predictions for the Q^2-dependence of form factors in neutrino reactions. A first and preliminary comparison indicates that the predictions are remarkably close to the data (Fig. 19). Another procedure is to try to extract from the data the moments of the x-distributions, which have a simpler Q^2-dependence than the distribution themselves according to QCD. Treating target mass

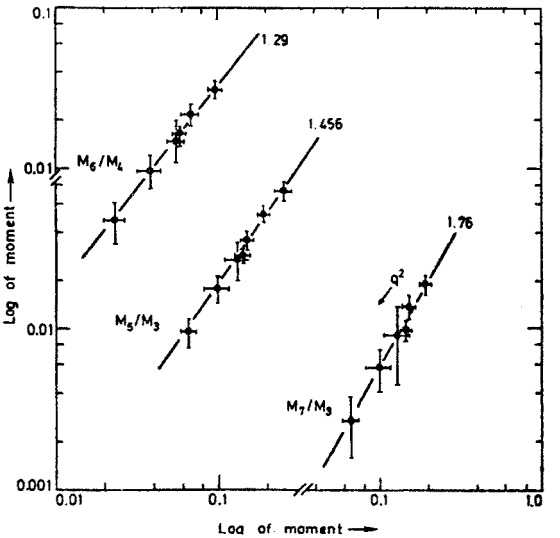

Fig. 20. Relation between moments of the valence quark distribution from BEBC–GGM. The slopes of the straight lines are the predictions of QCD

corrections according to the prescription of Nachtmann [23], the BEBC–GGM group have obtained moments of the valence quark distribution xF_3. The ratio between different moment shows exactly the Q^2-dependence required by QCD (Eq. (12), Fig. 20).

5. Summary and conclusions

Neutrino and antineutrino charged-current reactions give important, and in some respects unique, information on the structure of the nucleon. The present data can be very consistently interpreted in terms of the quark parton model. In particular,

(*i*) the Callan–Gross relation, derived from the assumption of spin $\frac{1}{2}$ particles, is valid within about 10%,

(*ii*) quarks and antiquarks carry about 45% of the nucleon momentum (antiquarks alone about 5.5%),

(*iii*) the distribution of antiquarks is concentrated at small x and approaches the distribution of quarks near $x = 0$,

(*iv*) neutrino and antineutrino cross-sections are equal at $y = 0$ within the flux uncertainties.

Dimuon events provide an interesting confirmation of these ideas. Their x-distributions are different from those of average charged current reactions, and agree well with the specific mixture of quark and antiquark distributions required in the standard model of charmed particle production.

The form factors exhibit deviations from scaling, at low Q^2 more than at high Q^2. This reflects, for example, in a drop of the neutrino cross-section per unit energy (σ/E) from low (< 10 GeV) to high (< 50 GeV) energies. The observed scaling deviations seem to be in quantitative agreement with expectations from QCD.

The comparison of neutrino and electron scattering data at the same Q^2 gives information about the ratio between the electric and weak charges of the quarks. Agreement within about 10% with the predicted values is observed.

It is a special pleasure to thank Professors A. Białas, W. Czyż and K. Zalewski for their friendly hospitality in Zakopane.

This report summarizes the work of a large number of people. The author is especially indebted to his colleagues of the CDHS Collaboration with whom he shared the excitements and the difficulties of a major experiment.

REFERENCES

[1] J. Steinberger, *Neutrino Interactions*, *in* Proc. 1976 CERN School of Physics, Wépion, Belgium, 1976, CERN 76-20 (1976), p. 57.
[2] See, for example, the review article of C. H. Llewellyn-Smith, *Phys. Reports* **3C**, 261 (1972).
[3] J. D. Bjorken, *Phys. Rev.* **179**, 1547 (1969).
[4] C. G. Gallan, D. J. Gross, *Phys. Rev. Lett.* **22**, 156 (1969).
[5] See, for example, L. M. Sehgal, ANL Report HEP-PR-75-45 (1975).
[6] J. T. Friedmann, H. W. Kendall, *Annu. Rev. Nuclear Sci.* **22**, 203 (1972).
[7] M. Holder et al., *Nucl. Instrum. Methods* **148**, 235 (1978).
[8] M. Holder et al., *Nucl. Instrum. Methods* **151**, 69 (1978).
[9] H. Deden et al., *Nucl. Phys.* **B85**, 269 (1975).
[10] T. Eichten et al., *Phys. Lett.* **46B**, 274 (1973).
[11] P. C. Bosetti et al., *Phys. Lett.* **70B**, 273 (1977).
[12] P. C. Bosetti et al., Oxford University preprint 16/78, submitted to *Nucl. Phys.* B.
[13] B. C. Barish et al., *Phys. Rev. Lett.* **39**, 1595 (1977).
[14] T. Hansl et al., Paper presented at the 7th Internat. Conf. on Neutrino Physics and Astrophysics, Purdue, 1978; T. Hansl et al., Paper presented at the Topical Conf. on Neutrinos at Accelerators, Oxford University, 1978.
[15] A. J. Buras, *Nucl. Phys.* **B125**, 125 (1977).
[16] M. Holder et al., *Phys. Lett.* **69B**, 377 (1977).
[17] B. C. Barish et al., *Phys. Rev. Lett.* **39**, 741 (1977).
[18] B. C. Barish et al., *Phys. Rev. Lett.* **40**, 1414 (1978).
[19] E. M. Riordan et al., SLAC-PUB 1634 (1975).
[20] A. J. Buras, K. J. F. Gaemers, *Nucl. Phys.* **B132**, 249 (1978).
[21] M. Glück, E. Reya, *Phys. Rev.* **D14**, 3034 (1976).
[22] H. L. Anderson et al., *Phys. Rev. Lett.* **40**, 1061 (1978).
[23] O. Nachtmann, *Nucl. Phys.* **B63**, 237 (1973); *Nucl. Phys.* **B78**, 455 (1974).